Progress In Electromagnetics Research C, Vol. 80, 233–247, 2018

Determination of Surface and Sub-Surface Cracks Location in Beams Using Rayleigh Waves

Atef Eraky[1], Rania Samir[1], Walid S. El-Deeb[2, *], and Abdallah Salama[1]

Abstract—Structural buildings are vulnerable to many types of damages that can occur through their life period. These damages may cause structure failure or at least decrease its efficiency. Dangerous damages occurring in concrete structures are surface opening cracks or sub-surface cracks. So, the determination of location of these cracks is very important, because the crack location is one of the important factors that affect the degree of danger of the damage. The Rayleigh waves have many advantages, as they can be easily recognized due to the maximum energy of the wave components. So, it was used to determine the crack location in the previous works. In this paper, two different techniques are used to determine the crack location; one of them depends on the healthy case, and the other deals only with the cracked case. Common finite element software (Abaqus) is used to model the numerical simulation, and the experimental test is also performed to verify the obtained numerical results. Good agreement between the simulated and experimental results is obtained by employing both techniques to find the crack location.

1. INTRODUCTION

Most damages spread in concrete structures are surface opening cracks and sub-surface cracks. These damages may be caused due to overloading, differential settlement, shrinkage, chemical attack, or temperature variation. The process of damage detection consists of many steps such as determination of damage location and determination of damage severity. The step of determination of the crack location is very important to know the degree of the danger of crack and also to detect the repair area, if the decision of the damage repair is chosen.

To detect the damage, lot of non-destructive testings (NDT) are used such as ultrasonic techniques, visual inspection, eddy current method, radiography methods, acoustic emission, magnetic methods, and stress waves methods. Recently, the Rayleigh wave (one of stress wave components) is used in NDT for concrete structures for many advantages as containing maximum energy of wave components [1, 2], which makes it recognized easily and propagates for large distances. The propagation of Rayleigh surface waves was studied on samples of aluminum, granite and mortar as part of a continuing effort to characterize Rayleigh waves in undamaged and damaged concrete [3].

A method using transient elastic wave tests was developed to scan the surface cracks of reinforced concrete. In the tests, an impact was applied at constant intervals along one side of the crack opening, and the surface response of the concrete due to each impact was measured and recorded. The procedure was repeated with the source applied on the opposite side. The method of ellipse intersection was adopted to process the surface response of the concrete structure [4]. An active sensing system with integrated actuators/sensors was controlled to excite and receive Lamb waves in the plate. Scattered wave signals from the damage were obtained by subtracting the baseline signal of the undamaged plate

Received 16 October 2017, Accepted 16 January 2018, Scheduled 25 January 2018

* Corresponding author: Walid S. El-Deeb (wseldeeb@ucalgary.ca).

[1] Department of Structural Engineering, Faculty of Engineering, Zagazig University, Zagazig, Egypt. [2] Department of Electronics and Communications Engineering, Faculty of Engineering, Zagazig University, Zagazig, Egypt.

from the recorded signal of the damaged plate [5]. Location identification of the closed micro-cracks in plate structures was achieved using the transient identification method based on Duffing oscillator. This method aimed to overcome the noise sensitivity, envelope fluctuation, weak energy, and uncertainty of mode conversion from reflection and transmission caused by the interaction between nonlinear Lamb wave and micro cracks [6, 7]. The loss of reciprocity in ultrasonic waves propagation was exploited as an imaging tool for localized cracks detection [8]. A numerical simulation and verification of health monitoring of beam structures is presented using propagating piezo-actuated lamb waves. The location of a linear crack in a beam is detected using an impact hammer and a piezoelectric sensor, based on the time-of-flight method [9].

An integral formulation was developed to predict Rayleigh wave emitted from a crack under stress combining Rayleigh wave, Green function and the crack opening displacement obtained from a fracture mechanic's model [10]. The use of Rayleigh waves was examined for the detection and sizing of surface-breaking cracks in concrete members. First, finite element simulations were performed to define the conditions for Rayleigh wave propagation in members with rectangular cross-section followed by an experimental study of a concrete beam [11–13]. Also, the vertical cracks in asphalt layers were detected using Rayleigh waves [14].

Acoustic wave propagation in materials containing internal frictional cracks was simulated in order to fully understand the microscopic behavior of contact defects and to predict their macroscopic nonlinear response [15]. The feasibility of impact generated Rayleigh waves for measuring deep surface opening cracks in concrete structures was studied [16]. The severity of different damages was studied using Rayleigh waves [17, 18]. The Bayesian inference approach was applied to conduct uncertainty quantification on notch damage in a beam structure using guided Lamb wave responses. The quantified associated uncertainties of these inferred values and the correlation between crack location and its extent is investigated, as well [19].

In this paper, the location of surface and sub-surface cracks is determined using two different techniques; one of them depends on the healthy case, and the other needs only the cracked case. The Rayleigh wave component is used in this study, due to its advantages. This wave is created using impact load with different frequencies from 10 kHz up to 50 kHz. Finite element software (Abaqus) is used to simulate the model, and the experimental test is also performed to verify the obtained numerical results.

2. RAYLEIGH WAVES

The propagation of stress wave can be defined as a linear deformation in a solid body under the action of a short-period transient force at the surface. Stress wave consists of many components: prim shear and Rayleigh waves. These components are divided into two categories: body waves (P-wave)

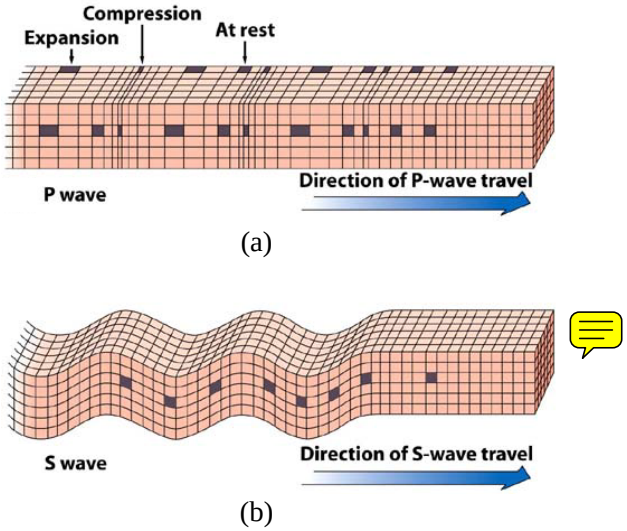

Figure 1. Waves propagation. (a) Primary waves. (b) Rayleigh (surface) waves.

and surface wave (S-wave).

The primary waves are longitudinal which cause the particles to oscillate in the direction of wave propagation as shown in Figure 1(a). They have the maximum speed in comparison with the other wave's components.

Rayleigh waves are the surface waves that propagate along the surface or interface of a solid medium. These waves cause the particles to move in elliptical manner such that the surface appears to be moving in up and down motion as shown in Figure 1(b).

The Rayleigh waves have many advantages as ithey can be recognized easily because they contain the maximum energy of the wave components. Rayleigh waves have influence on the body surface and sub-surface and their influence is clear until depth equal its wavelength as shown in Figure 2.

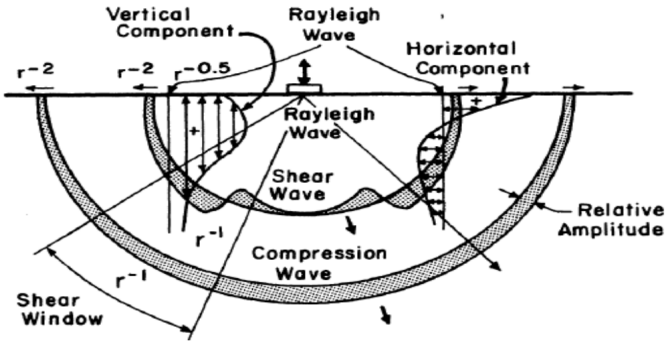

Figure 2. Energy distribution of stress waves [1].

3. MODELING AND THEORY

A common finite element program (Abaqus) is used to simulate the propagation of stress waves. To study the problem, the dynamic explicit method is used. In studying the wave propagation using finite element, the element size and time increment must be chosen carefully to avoid the error in simulation. At least 10 elements are needed to simulate one wavelength (λ), so the element size (l) can be chosen as function of the number of elements (n), which ranges from 10 to 20 according to Equation (1), and the time increment (Δt) can be chosen according to Equation (2) based on wave velocity (c) as follows [1]:

$$l = \frac{\lambda}{n} \tag{1}$$

$$\Delta t = \frac{l}{c} \tag{2}$$

The simulation of problem is done in 2-D as shown in Figure 3. The stress waves are created at assumed origin point by impact load. There are four sensors employed in this model. Two of them are located at $X1$ and $X2$ distances on the right side of the impact load which represents the cracked side. The other two are located on the left side of the impact load, which represents the healthy side. The crack is located at x_3 from the impact load.

During an impact, using collision of steel sphere in the concrete surface, a portion of the potential energy in the sphere is transferred to the elastic wave energy in the structure which causes particle displacements. In the case of concrete, a mechanical impact source is normally used to generate a stress pulse with sufficient acoustic energy to overcome the effects of attenuation and divergence [1].

A half sine wave or half cubic sine wave can be used to simulate the impact load according to Equations (3) and (4) [1].

$$F(t) = F_{\max} \times \sin\left(\frac{\pi t}{t_c}\right) \tag{3}$$

$$F(t) = F_{\max} \times \sin^3\left(\frac{\pi \times t}{t_c}\right) \tag{4}$$

where $F_{\max}$ is the maximum amplitude and t_c is the time contact.

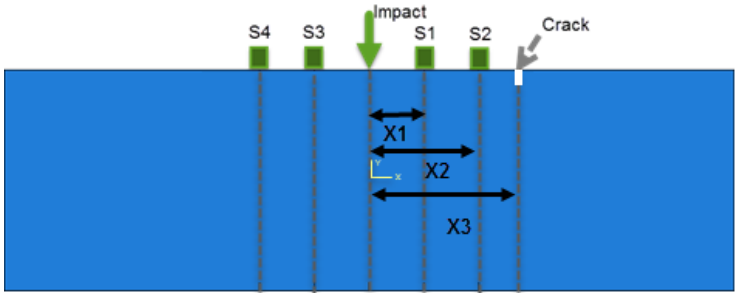

Figure 3. Model of the tested beam.

4. PROPOSED TECHNIQUES

4.1. The First Technique

In the first technique, the data are obtained from sensors that are located at distances $X1$ and $X2$ for both cracked and healthy sides. The Hilbert transform is applied to get the time of flight of Rayleigh wave (T_1 and T_2). The time of reflected wave is obtained from the difference between the two cases as shown in Figure 4 and Figure 5. The speed of Rayleigh wave and the speed of reflected wave are calculated using Equations (5) and (6), respectively. Then, the average speed is obtained, and finally the crack location is detected using Equation (7). Figure 8 shows the flowchart of first technique.

$$C_R = \frac{X2 - X1}{T_2 - T_1} \tag{5}$$

$$C_{Rref} = \frac{X2 - X1}{T_{2ref} - T_{1ref}} \tag{6}$$

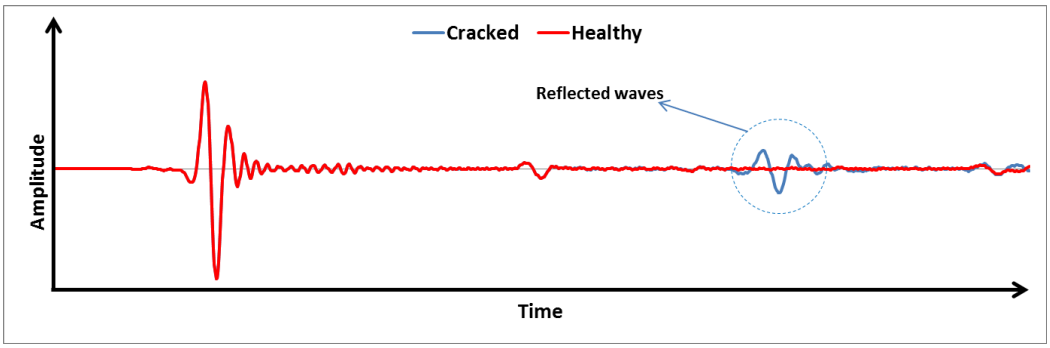

Figure 4. Wave signals of cracked and healthy cases.

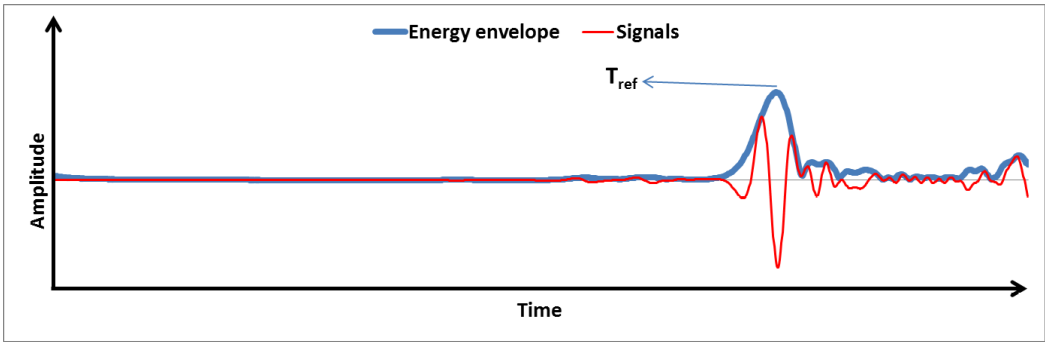

Figure 5. Wave signals and energy envelope of the difference between cracked and healthy cases.

$$X3 = X1 + \frac{(C_R + C_{Rref})}{2} \times \frac{(T_{1ref\_}T_1)}{2} \tag{7}$$

4.2. The Second Technique

The second technique requires the data of the wave from the cracked case only. It can determine the crack location by using permutations to recognize the reflected wave. So, in the second technique the same steps used in the first technique can be followed, but the time of flight of the reflected waves can be determined using permutations of maximum peaks. The maximum peak is determined for each sensor as shown in Figure 6. Every peak of the signal of sensor $S1$ is studied with all peaks of sensor $S2$ individually to get the speed of the reflected wave as shown in Figure 7. Then, the crack location for both sensors is calculated using Equations (8) and (9).

$$X31 = X1 + 0.5 \times (T_{1ref\_}T_1) \times v_{average} \tag{8}$$

$$X32 = X2 + 0.5 \times (T_{2ref\_}T_2) \times v_{average} \tag{9}$$

where: $X31$ and $X32$ are the crack locations by sensors $S1$ and $S2$, respectively; T_{1ref} and T_{2ref} are the time periods of the assumed peaks for the two trials; $v_{average}$ is the average speed of the signal.

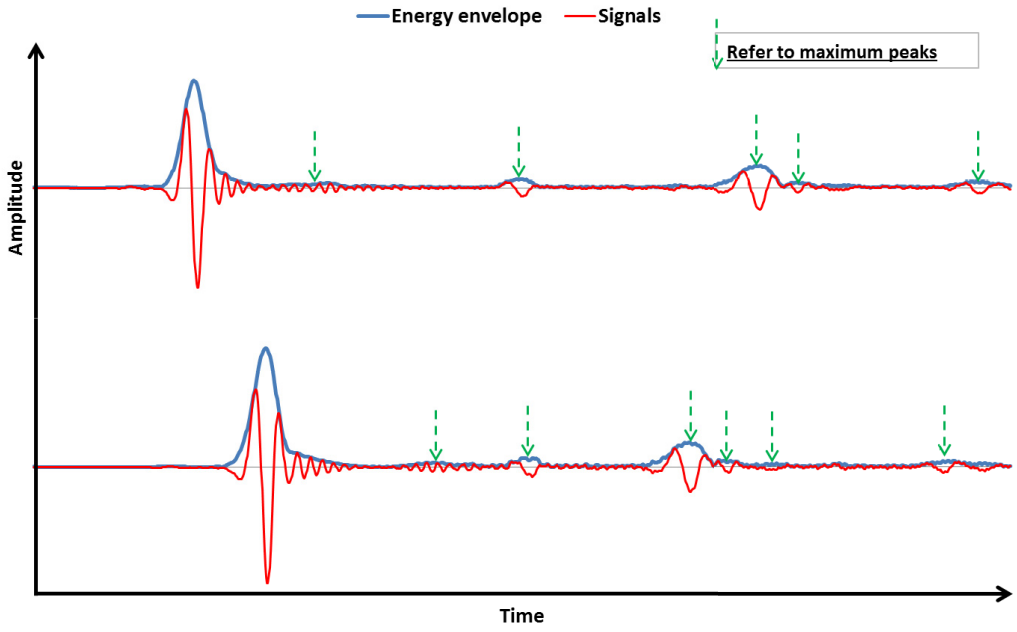

Figure 6. Maximum peaks of sensors $S1$ and $S2$.

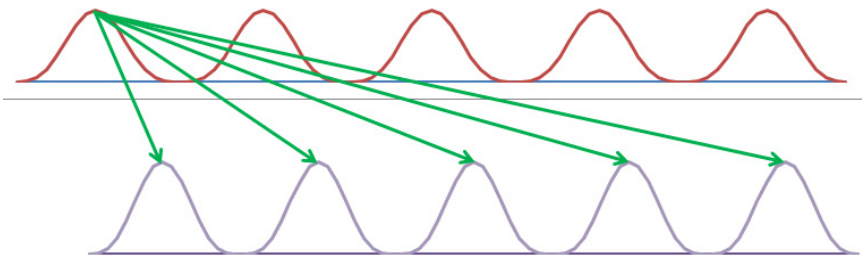

Figure 7. Permutations of sensors peaks.

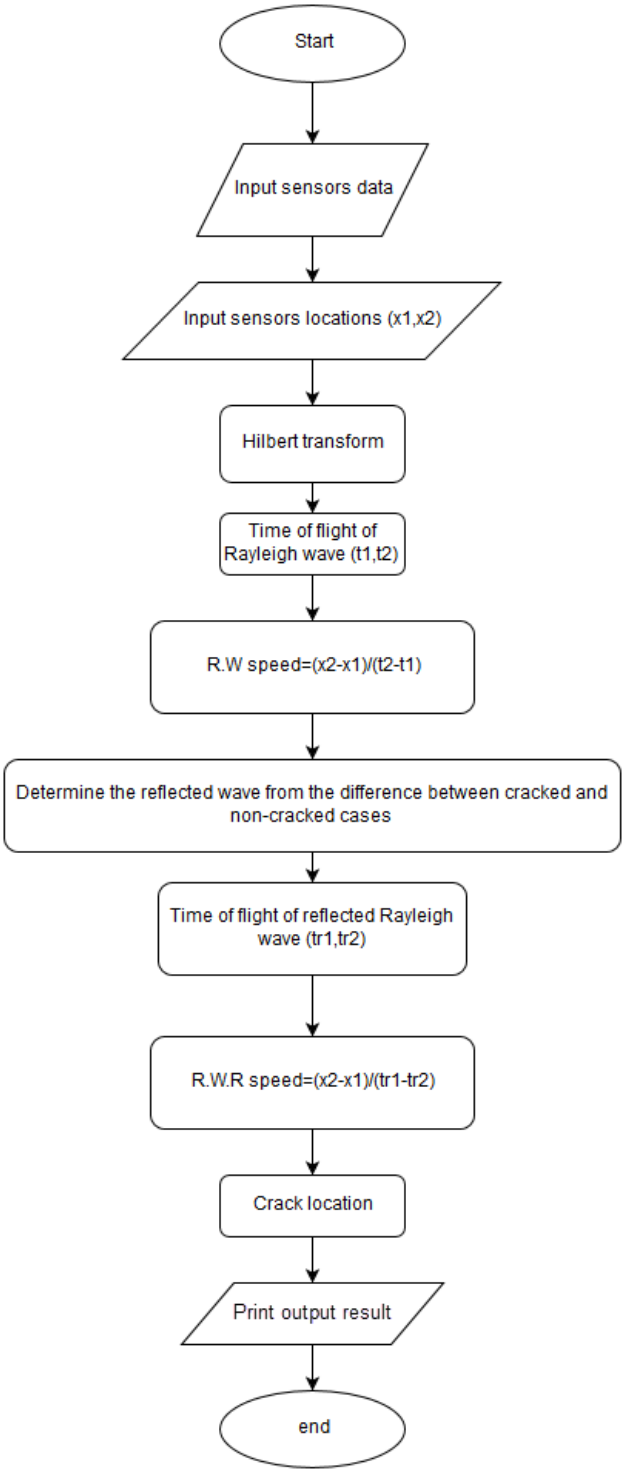

Figure 8. Flowchart of the first technique.

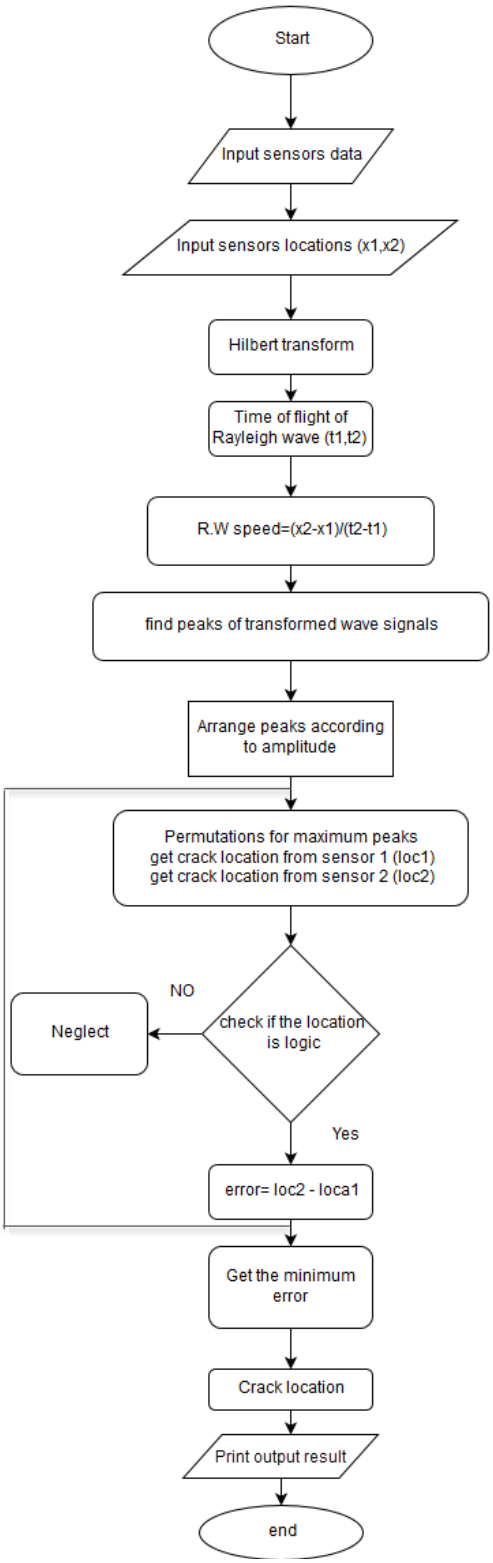

Figure 9. Flowchart of the second technique.

Some peaks are rejected for some of the following conditions. Firstly, the time of the reflected wave from sensor $S2$ is larger than the time of reflected wave from sensor $S1$, because the reflected wave passes by sensor ($S2$) firstly. Secondly, the speed of the reflected wave is an unexpected value. The error between the two locations which are detected by the two sensors is determined using Equation (10).

$$Error = X31 - X32 \tag{10}$$

The error between the two locations is estimated for each step. The minimum error indicates the final crack location. Figure 9 shows the flowchart of the second technique.

5. SIMULATION RESULTS

5.1. Determination of Surface Crack Location

Surface cracks location in plain concrete beam with dimensions (200 cm length and 60 cm depth) is studied using generated impact load with different wave frequencies starting from 10 KHz up to 50 KHz as shown in Figure 10. Also, different sensor locations are studied for ($X1 = 20$ cm, $X2 = 30$ cm), ($X1 = 20$ cm, $X2 = 40$ cm), and ($X1 = 30$ cm, $X2 = 40$ cm) to verify the ability of the proposed techniques to detect the crack at different sensor locations. The sensors detect the vertical acceleration at these locations, and the data are sent to the PC to be analyzed using Matlab software by applying the two proposed techniques. The actual location of the crack is 60 cm from the impact point for both surface and sub-surface cases.

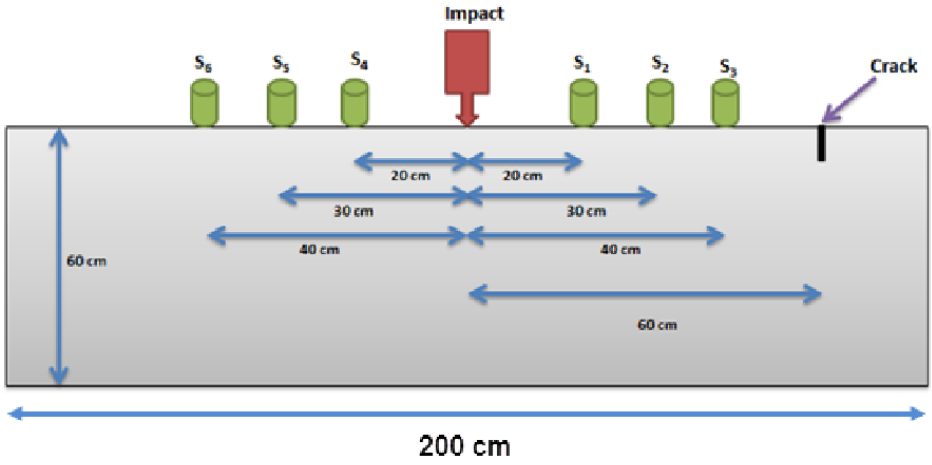

Figure 10. Beam with surface crack model.

In surface case, the vertical crack depth is assumed 4 cm, and for sub-surface case, the crack is located at 4 cm from the surface with 4 cm depth, as well. The properties chosen for concrete are shown in Table 1.

Table 1. Concrete properties for beam model.

Item	Value
Mass Density	2200 kg/m^3
Poisson Ratio	0.2
Modulus of Elasticity	26.2 Gpa

Figure 11 shows the actual and estimated surface crack locations using first technique at different wave frequencies and at sensors locations ($X1 = 20$ cm, $X2 = 30$ cm), as an illustrative case. It has been observed that the first technique has a good ability for determining the crack location in the surface

case. The percentage of error in estimating the crack location is higher with low frequencies but still in acceptable range where the maximum error of 1.17% is obtained. This is because the low frequency wave has long wavelength, and the penetration of Rayleigh waves increases with increasing the wavelength. So, the amount of the reflected wave energy is low, especially when the crack depth is small.

Figure 12 shows the actual and estimated surface crack locations by employing the second technique at different wave frequencies and at sensors locations ($X1 = 20\,\text{cm}$, $X2 = 30\,\text{cm}$), as an illustrative case.

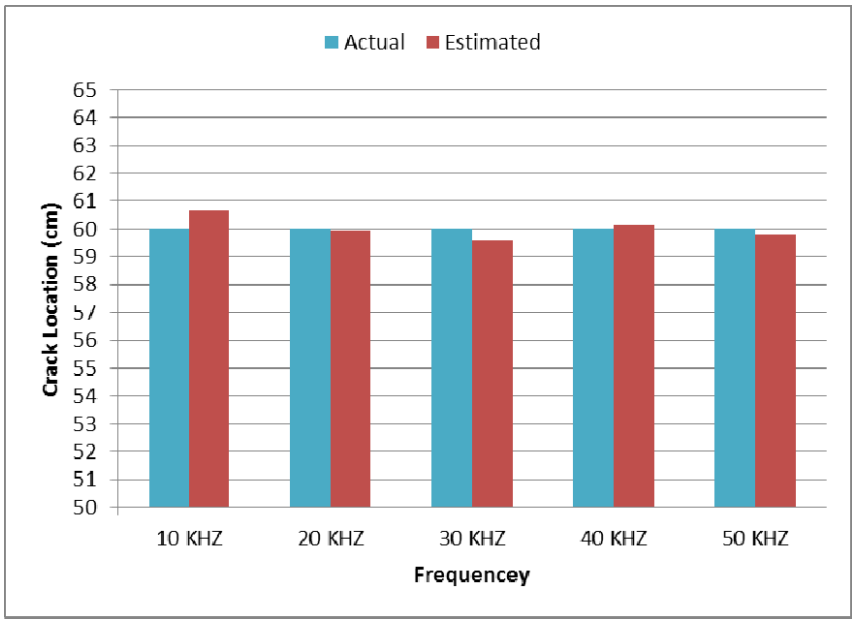

Figure 11. Surface crack location with different wave frequencies using the first technique for ($X1 = 20\,\text{cm}$, $X2 = 30\,\text{cm}$).

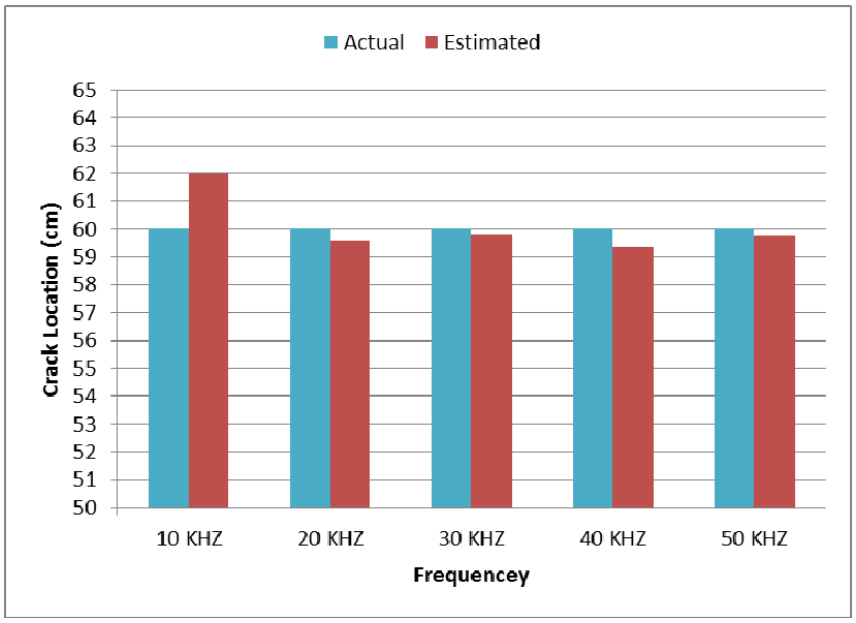

Figure 12. Surface crack location with different wave frequencies using the second technique for ($X1 = 20\,\text{cm}$, $X2 = 30\,\text{cm}$).

It is shown that the second technique has a good ability for determining the crack location in the surface case. The percentage of error in estimating the crack location is higher in low frequencies with maximum error of 3.33%.

Table 2 shows the estimated surface crack location by employing the first and second techniques at different wave frequencies and at different sensors locations. It has been noticed that both techniques have a good ability for determining the crack location in the surface case, and the percentage of error in estimating the crack location is higher with low frequencies. In the first technique, it is noticed that the cracks are detected more accurately when the two sensors are located far from the crack.

Table 2. Detected surface crack location in (cm) with different wave frequencies using first and second techniques at different sensors locations ($X1$ and $X2$).

Frequency (KHz)	X1=20 cm, X2=30 cm		X1=20 cm, X2=40 cm		X1=30 cm, X2=40 cm	
	First Technique	Second Technique	First Technique	Second Technique	First Technique	Second Technique
10	60.68	61.98	61.16	61.41	61.41	59.99
20	59.94	59.57	60.22	59.71	60.36	60.43
30	59.6	59.8	59.92	59.56	60.09	59.45
40	60.12	59.38	59.88	59.38	59.76	60.03
50	59.83	59.76	59.88	59.76	59.9	60.17

Table 3 shows the percentage error of detecting surface crack location for the first and second techniques at different sensors locations. It is found that the percentage error of the first and second techniques in detecting the surface crack does not exceed 3.3%. Overall, the two techniques detect the crack location with acceptable error for all cases of sensors locations. The percentage of error in estimating the crack location is higher with low frequencies. In the first technique, it is noticed that the cracks are detected more accurately when the two sensors are located far from the crack, i.e., ($X1 = 20$ cm, $X2 = 30$ cm), while in the second technique, it is noticed that the cracks are detected more accurately when the two sensors are near the crack, i.e., ($X1 = 30$ cm, $X2 = 40$ cm). The second technique detects the crack location accurately when the sensors are located at distances ($X1 = 20$ cm, $X2 = 40$ cm) with maximum error of 2.35%. The accuracy increases when the sensors are located at distances ($X1 = 30$ cm, $X2 = 40$ cm) with maximum error of 0.92%.

Table 3. Percentage error of first and second techniques for detecting surface crack location with different wave frequencies at different sensors locations ($X1$ and $X2$).

Frequency (KHz)	X1=20 cm, X2=30 cm		X1=20 cm, X2=40 cm		X1=30 cm, X2=40 cm	
	First Technique	Second Technique	First Technique	Second Technique	First Technique	Second Technique
10	1.13%	3.30%	1.93%	2.35%	2.35%	0.02%
20	0.10%	0.72%	0.37%	0.48%	0.60%	0.72%
30	0.67%	0.33%	0.13%	0.73%	0.15%	0.92%
40	0.20%	1.03%	0.20%	1.03%	0.40%	0.05%
50	0.28%	0.40%	0.20%	0.40%	0.17%	0.28%

5.2. Determination of Sub-Surface Crack Location

The first technique is applied to detect the sub-surface crack with different wave frequencies when the sensors are located at different distances, as done before in the case of surface crack location. It is found that the first technique detects the crack location with maximum error of 5.4% for sensors located at distances ($X1 = 20$ cm, $X2 = 30$ cm), as shown in Figure 13 as an illustrative case.

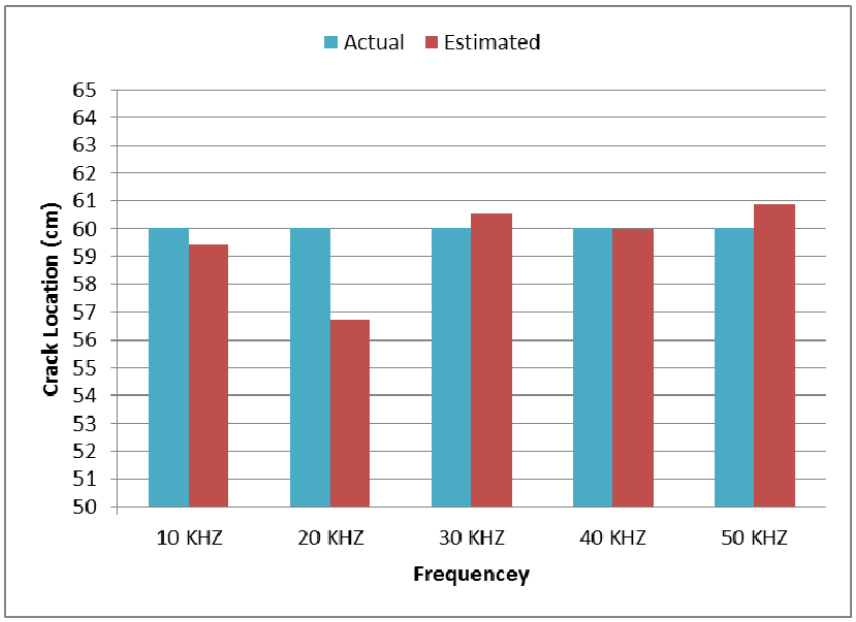

Figure 13. Sub-surface crack location with different wave frequencies using the first technique for ($X1 = 20\,\text{cm}$, $X2 = 30\,\text{cm}$).

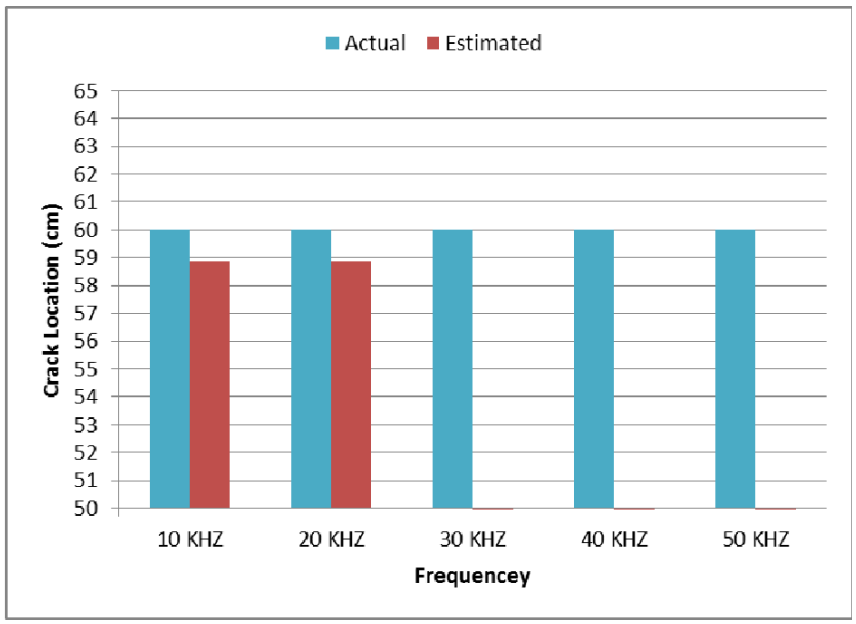

Figure 14. Sub-surface crack location with different wave frequencies using the second technique for ($X1 = 20$, $X2 = 30$).

Figure 14 shows the actual and estimated sub-surface crack locations using the second technique at different wave frequencies with sensors located at ($X1 = 20\,\text{cm}$, $X2 = 30\,\text{cm}$), as an illustrative case. It is found that the second technique cannot detect the location of the sub-surface cracks in high frequency waves.

Table 4 shows the estimated sub-surface crack location by employing the first and second techniques at different wave frequencies and at different sensors locations. Table 4 also shows that the second technique has limitation in estimating the sub-surface crack location in the cases of high frequencies.

Table 4. Detected sub-surface crack location in (cm) with different wave frequencies using first and second techniques at different sensors locations ($X1$ and $X2$).

Frequency (KHz)	X1=20 cm, X2=30 cm		X1=20 cm, X2=40 cm		X1=30 cm, X2=40 cm	
	First Technique	Second Technique	First Technique	Second Technique	First Technique	Second Technique
10	59.43	58.88	59.65	59.77	59.77	57.67
20	56.75	58.87	58.94	59.74	60.27	59
30	60.56	---	57.55	---	56.57	---
40	59.99	---	57.54	---	56.7	---
50	60.88	---	57.21	---	56.14	---

This is because the wavelength of high frequency waves is small which means low penetration for Rayleigh wave. So, the reflection from the sub-surface cracks is very small, and the second technique cannot recognize it. In contrast, with low frequency cases, the wavelength is large enough to allow more penetration for the Rayleigh wave. So, the amount of reflected energy is recognized using the second technique with low frequency waves.

Table 5 shows the percentage error of detecting sub-surface crack location for the first and second techniques at different sensors locations. It is found that the maximum error of 4.65% is obtained when using the first technique in detecting sub-surface crack for sensors locations of ($X1 = 20\,\text{cm}$, $X2 = 40\,\text{cm}$), and the maximum error of 6.4% is also obtained for sensors locations of ($X1 = 30\,\text{cm}$, $X2 = 40\,\text{cm}$).

Table 5. Percentage error of first and second techniques for detecting sub-surface crack location with different wave frequencies at different sensors locations ($X1$ and $X2$).

Frequency (KHz)	X1=20 cm, X2=30 cm		X1=20 cm, X2=40 cm		X1=30 cm, X2=40 cm	
	First Technique	Second Technique	First Technique	Second Technique	First Technique	Second Technique
10	0.95%	1.87%	0.58%	0.38%	0.38%	3.88%
20	5.42%	1.88%	1.77%	0.43%	0.45%	1.67%
30	0.93%	---	4.08%	---	5.72%	---
40	0.02%	---	4.10%	---	5.50%	---
50	1.47%	---	4.65%	---	6.43%	---

It is observed that the maximum error for the first technique in detecting the sub-surface cracks is higher than that in the case of surface cracks. This is because the first technique depends on comparing the reflected wave in the healthy side and the cracked side, and in the case of sub-surface cracks, a part of wave energy passes over the sub-surface crack, and the reflected part is lower than that reflected in case of surface crack.

It is also noticed that in the case of low frequency waves, the second technique detects sub-surface crack location more accurately when the two sensors are located at far distances from each other, i.e., ($X1 = 20\,\text{cm}$, $X2 = 40\,\text{cm}$).

Table 6 shows a comparison between Rayleigh wave's method and the other techniques used in the process of damage detection. It is clear from the previous results that the proposed two techniques get good estimation for the detection of surface and sub-surface cracks compared with the previous researches.

Table 6. Comparison between employing the Rayleigh wave method and other techniques for determination of the crack locations.

Reference	Technique	Samples	Type of Cracks	Percentage Error
Dimitrina [20]	Vibration based method	Simply supported beam	Surface Cracks	0.2–8.2%
Xiaofeng [6]	Duffing oscillator transient transition	Aluminum plates	Internal Cracks	1.3–3.3%
Li, B. [21]	wavelet finite element methods	Steel beam	Surface Cracks	0.2–24.8% 0.1–9.9% for elastic modulus correction
Mehta, P. [22]	Signal Processing and Strain Energy Based Model	Cantilever beam	Surface Cracks	0.00–9%
Yong, J. [23]	Wavelet Transform and Fractal Dimension	Steel cantilever beam	Surface Cracks	2.5–10%
This research	Rayleigh waves	Plain concrete beam	Surface and Sub-Surface Cracks	0.02–3.3% for surface cracks 0.02–6.5% for sub-surface cracks

6. EXPERIMENTAL RESULTS

To verify the applicability of the two techniques on the realistic structures, a plain concrete beam is tested experimentally. This beam simulates the real beam in structures, although it is rested on the floor and does not have supports. However, this does not affect the results because these techniques depend on the oscillation of the materials particles not the vibration of the whole structures. Also, the loads on the realistic beams could be ignored because these loads do not affect the reflected waves from the cracks which are used to estimate the locations of cracks.

The model of the experimental works is a plain concrete beam with dimensions (160 cm length, 12.5 cm width, and 25 cm height). The tools and instruments of the experimental test shown in Figure 15 are described as follows:

- Hammer: to generate the impact loads on the surface of cracked beam. The frequency of steel hammer ranges from 2 to 4.8 kHz.
- B&K accelerometer sensors (model 4369): to detect the vertical acceleration at the sensor location and send it to the oscilloscope.
- Tektronix 2024 oscilloscope: to convert the data from the sensors to signals and monitor it on the screen and send the data to the personal computer. The time per division of the oscilloscope is chosen according to the beam length and the speed of the wave. It should be adjusted to show the time of the incident and reflected waves for the crack.
- Personal computer: to analyze the data and detect the crack location by using the two proposed techniques that are compared to the simulation results.

Figure 15. B&K accelerometer sensors and Tektronix 2024 oscilloscope.

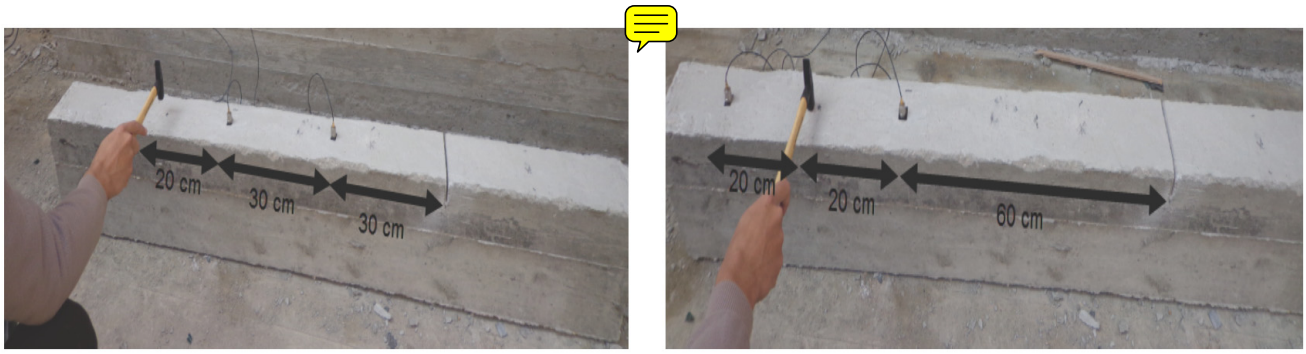

(a) (b)

Figure 16. Experimental test. (a) The first technique. (b) The second technique.

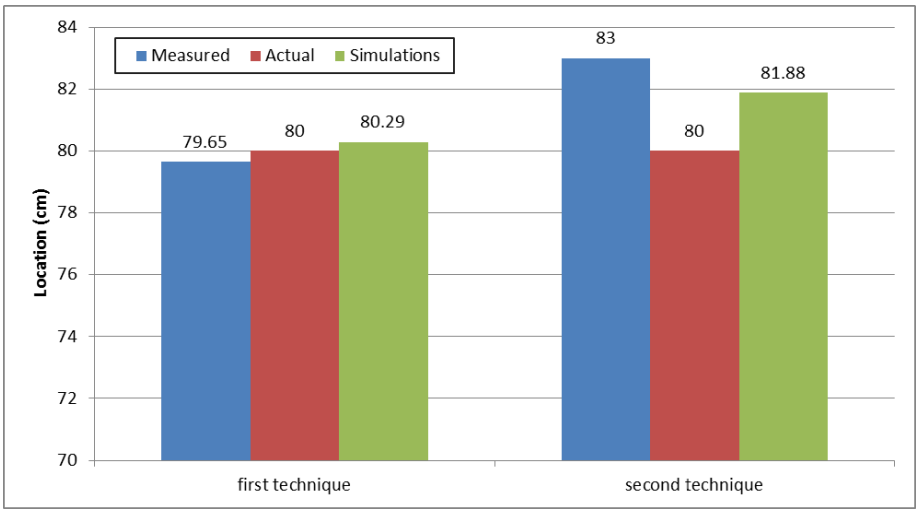

Figure 17. Surface crack location for the simulations and the experimental test.

The crack is located at 80 cm distance from impact load. Figures 16(a) and (b) show the distances between the sensors and the surface crack for the first and second techniques, respectively.

Figure 17 shows the results obtained by employing the first and second techniques from the simulations and experimental works. The results prove that both techniques are able to detect the surface crack accurately.

7. CONCLUSION

A finite element program (Abaqus) is used in this study for simulating the Rayleigh wave's propagation in concrete beams. Two techniques are used to detect the surface and sub-surface crack location at different locations with different waves frequencies. Verification is done with experimental work to show the accuracy of the two proposed techniques.

Rayleigh waves are a good stress wave component for studying the surface and sub-surface crack location due to its high energy and the ability to be recognized easily. The first technique, which depends on the information of cracked and healthy cases, gives good results in both surface and sub-surface cases. The second technique, which depends on the information of the cracked case only, gives good results in the surface case, but it has a limitation in the sub-surface case.

Low frequency waves are better than high frequency waves for estimating the sub-surface crack location especially in the second technique. This is due to their ability of high penetration, which depends on the wavelength. The location of the sensors does not affect the estimation of the crack location except in the case of detecting the sub-surface crack. With low frequency waves, the second technique detects the sub-surface crack location more accurately when the two sensors are located at far distance from each other.

REFERENCES

1. Lee, Y. H. and T. Oh, "The measurement of P-, S-, and R-wave velocities to evaluate the condition of reinforced and prestressed concrete slabs," *Advances in Materials Science and Engineering*, Vol. 2016, 14 pages, Article ID 1548215, 2016, doi:10.1155/2016/1548215.
2. Rix, G., C. Lai, and S. Foti, "Simultaneous measurement of surface wave dispersion and attenuation curves," *Geotechnical Testing Journal*, Vol. 24, No. 4, 350–358, 2001.
3. Joseph, O. and J. Laurence, *Characterization of Rayleigh Wave Propagation in Concrete Using Laser Ultrasonic*, Springer, 1998.
4. Liu, P. L., K. H. Lee, T. T. Wu, and M. K. Kuo, "Scan of surface-opening cracks in reinforced concrete using transient elastic waves," *NDT & E International*, Vol. 34, No. 3, 219–226, 2001.
5. Lei, W. and F. G. Yuan, "Active damage localization technique based on energy propagation of Lamb waves," *Smart Structures and Systems*, Vol. 3, No. 2, 201–217, 2006.
6. Liu, X., L. Bo, Y, Liu, Y. Zhao, J. Zhang, N. Hu, and M. Deng, "Location identification of closed crack based on Duffing oscillator transient transition," *Journal of Sound and Vibration*, Vol. 100, 384–397, 2017.
7. Liu, X., L. Bo, Y, Liu, Y. Zhao, J. Zhang, N. Hu, and M. Deng, "Detection of micro-cracks using nonlinear lamb waves based on the Duffing-Holmes system," *Journal of Sound and Vibration*, Vol. 406, 175–186, 2017.
8. Scalerandi, M., S. Gliozzi, and C. Bruno, "Detection and location of cracks using loss of reciprocity in ultrasonic waves propagation," *Journal of the Acoustical Society of America*, Vol. 131, EL81, 2012.
9. Soorgee, M. H. and K. A. Yousef, "Crack diagnosis in beams using propagated waves and Hilbert Huang transformation," *4th International Conference on NDT*, Hellenic Society for NDT, China, Crete Greece, 2007.
10. Ben Khalifa, W., K. Jezzine, and S. Grondel, "3D modeling of Rayleigh wave acoustic emission from a crack under stress," *Acoustics 2012 Nantes Conference*, French Acoustic Society, paper 000593, 2627–2632, 2013.

11. Moser, F., L. Jacobs, and J. Qu, "Modeling elastic wave propagation in waveguides with the finite element method," *NDT & E International*, Vol. 32, 225–234, 1999.
12. Olsson, D., "Numerical simulations of energy absorbing boundaries for elastic wave propagation in thick concrete structures subjected to impact loading," Master of Science Thesis, Umea University, 2012.
13. Zerwer, A., M. A. Polak, and J. C. Santamarina, "Detection of surface breaking cracks in concrete members using rayleigh waves," *Journal of Environmental and Engineering Geophysics, JEEG*, Vol. 10, No. 3, 295–306, September 2005.
14. Iodice, M., J. Muggleton, and E. Rustighi, "The detection of vertical cracks in asphalt using seismic surface wave methods," *Journal of Physics: Conference Series*, 744, 2016.
15. Delrue, S. and V. Aleshin, "2D modeling for acoustic waves in solids with frictional cracks," *23rd French Conference of Mechanics*, 2017.
16. Haw, K. C., M. Shohei, and S. Tomoki, "Characterization of deep surface opening crack in concrete," *ACI Material Journal*, Vol. 107, No. 3, 306–311, 2010.
17. Foo, W. L., S. L. Kok, and K. C. Hwa, "Determination and extraction of Rayleigh-waves for concrete cracks characterization based on matched filtering of center of energy," *Journal of Sound and Vibration*, Vol. 363, 303–315, 2016.
18. Foo, W. L., S. L. Kok, and K. C. Hwa, "Assessment of reinforced concrete surface breaking crack using Rayleigh wave measurement," *Journal of Sensors*, Vol. 16, No. 3, 337, 2016.
19. Gang, W., "Beam damage uncertainty quantification using guided Lamb wave responses," *Journal of Intelligent Material Systems and Structure*, special issue, DOI: 10.1177/1045389X17704911, 2017.
20. Dimitrina, K., "Vibration-based methods for detecting a crack in a simply supported beam," *Journal of Theoretical and Applied Mechanics*, Vol. 44, No. 4, 69–82, 2014.
21. Li, B., X. Chen, J. Ma, and Z. He, "Detection of crack location and size in structures using wavelet finite element methods," *Journal of Sound and Vibration*, Vol. 285, No. 5, 767–782, 2005.
22. Mehta, P., A. Kureshi, S. Lad, A. Patel, and D. Sharma, "Detection of cracks in a cantilever beam using signal processing and strain energy based model," *Materials Science and Engineering*, Vol. 234, 012008, doi:10.1088/1757-899X/234/1/012008, 2017.
23. Yong, J., L. Bing, Z. Zhou, and C. Xue, "Identification of crack location in beam structures using wavelet transform and fractal dimension," *Shock and Vibration*, Vol. 2015, Article ID 832763, 2015.

Errata to "Determination of Surface and Sub-Surface Cracks Location in Beams Using Rayleigh Waves"

by Atef Eraky, Rania Samir, Walid S. El-Deeb, and Abdallah Salama
in Progress In Electromagnetics Research C, Vol. 80, 233–247, 2018

Atef Eraky[1], Rania Samir[1], Walid S. El-Deeb[2, *], and Abdallah Salama[1]

1) Figure 1(b) listed as Rayleigh wave while the image is for Shear wave, and the correct image of the Rayleigh wave is shown in the following figure.

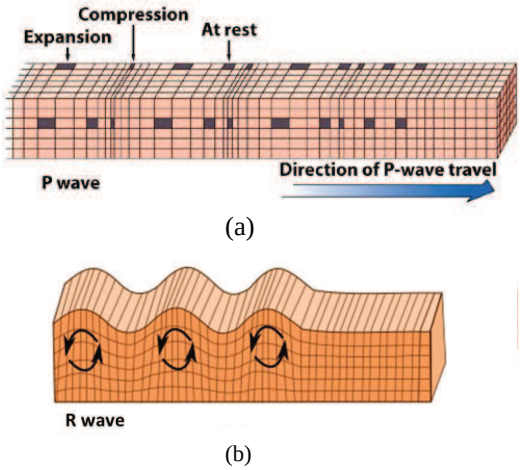

Figure 1. Waves propagation. (a) Primary waves. (b) Rayleigh (surface) waves.

2) In the text of the second section (2. Rayleigh Waves), in the second sentence of the first paragraph: These components are divided into two categories: body waves (P-wave) and surface wave (S-wave). However, the correct categories are: body waves (P-wave and S-wave) and surface wave (R-wave).
3) In Figure 16, the two subfigures ((a) & (b)) are reversed as follows.

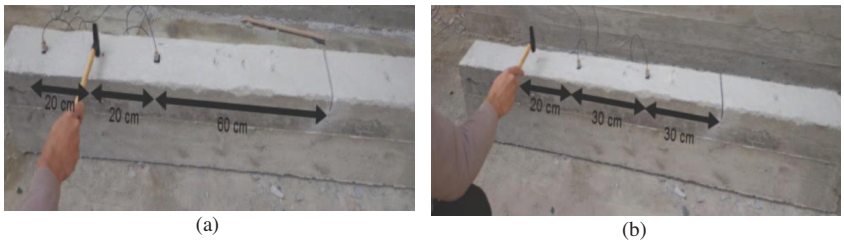

Figure 16. Experimental test. (a) The first technique. (b) The second technique.

Received 25 July 2018, Added 27 July 2018
* Corresponding author: Walid S. El-Deeb (wseldeeb@ucalgary.ca).
[1] Department of Structural Engineering, Faculty of Engineering, Zagazig University, Zagazig, Egypt. [2] Department of Electronics and Communications Engineering, Faculty of Engineering, Zagazig University, Zagazig, Egypt.